

# Harmonizing Covariance and Expressiveness for Deep Hamiltonian Regression in Crystalline Material Research: a Hybrid Cascaded Regression Framework

Shi Yin <sup>†1</sup> Xinyang Pan <sup>2</sup> Xudong Zhu <sup>1,2</sup> Tianyu Gao <sup>2</sup> Haochong Zhang <sup>1</sup> Feng Wu <sup>1,2</sup> Lixin He <sup>†1,2</sup>

## Abstract

Deep learning for Hamiltonian regression of quantum systems in material research necessitates satisfying the covariance laws, among which achieving SO(3)-equivariance without sacrificing the expressiveness of networks remains an elusive challenge due to the restriction to non-linear mappings on guaranteeing theoretical equivariance. To alleviate the covariance-expressiveness dilemma, we propose a hybrid framework with two cascaded regression stages. The first stage, with a theoretically-guaranteed covariant neural network modeling symmetry properties of 3D atom systems, yields theoretically covariant features and baseline Hamiltonian predictions, assisting the second stage in learning covariance. Meanwhile, the second stage, powered by a non-linear 3D graph Transformer network we propose for structural modeling of 3D atomic systems, refines the first stage’s output as a fine-grained prediction of Hamiltonians with better expressiveness capability. The combination of a theoretically covariant yet inevitably less expressive model with a highly expressive non-linear network enables precise, generalizable predictions while maintaining robust covariance under coordinate transformations. Our method achieves state-of-the-art performance in Hamiltonian prediction for electronic structure calculations, confirmed through experiments on five crystalline material databases.

## 1. Introduction

Currently, Density Functional Theory (DFT) (Hohenberg & Kohn, 1964; Kohn & Sham, 1965) stands as a cornerstone in the field of materials science, offering unparalleled insights into the properties of materials. Within this frame-

work, the Kohn-Sham Hamiltonian plays an essential role in understanding a wide range of material properties, including electronic structures, magnetic properties, optics, transport, and numerous other properties. However, obtaining the Hamiltonian through DFT involves complex and costly selfconsistent iterations, which have become a major bottleneck when applying this method to large-scale material systems. Recently, deep learning methods (Schütt et al., 2019; Unke et al., 2021; Gu et al., 2022; Li et al., 2022; Gong et al., 2023) have emerged as a promising trend for predicting Hamiltonians. These methods have demonstrated potential in terms of prediction accuracy and offer a way to bypass the computationally exhaustive self-consistent steps, thereby providing a viable pathway for the effective simulation of large-scale atomic systems.

However, applying deep learning techniques to the Hamiltonian prediction task continues to present substantial challenges. An accuracy to three decimal places of electronvolt, namely the milli-electronvolt (meV, namely  $10^{-3}$ eV) scale, is typically required, and an accuracy to the sub-meV ( $10^{-4}$ eV) scale, is welcomed, to achieve a satisfactory level of accuracy for calculating the down-stream physical quantities such as band structures. Furthermore, the fidelity of Hamiltonian predictions should not be confined to a specific coordinate system; rather, the results must demonstrate robust symmetry and generalizability and across various choices of reference frames. This necessitates that deep learning methods capture the intrinsic symmetries of the Hamiltonian with respect to transformations of the coordinate system, thereby ensuring the consistency with physical principles covariant to these transformations. In the context of Hamiltonian prediction, such covariance principles manifest as a combination of 3D translational invariance and rotational equivariance. By utilizing relative coordinates, translational invariance has been effortlessly achieved, while rotational equivariance, i.e., equivariance to the SO(3) group, remains a challenging target to guarantee. This difficulty arises because the Hamiltonian of each pair of atoms is usually high-dimensional, and its variation space under rotational operations is large. Consequently, it is difficult to cover the vast variability space they inhabit merely depending on discrete training samples. To address this, several works, such as DeepHE3 (Gong et al., 2023), applied group

<sup>1</sup>Institute of Artificial Intelligence, Hefei Comprehensive National Science Center <sup>2</sup>University of Science and Technology of China. Correspondence to: Shi Yin <shiyin@iai.ustc.edu.cn>, Lixin He <helx@ustc.edu.cn>.

theory-guaranteed covariant feature descriptors and tensor operators enabling the assurance of  $SO(3)$ -equivariance directly at the network mechanism level. However, to theoretically guarantee strict rotational covariance, these methods did not permit the use of any non-linear activation layers for  $SO(3)$ -equivariant features. Given that the expressiveness capability of modern deep networks heavily relies on the extensive use of non-linear mappings, this restriction resulted in a significant curtailment of the network’s expressiveness capabilities. This, in turn, led to bottlenecks in fitting complex mappings, which ultimately caps the accuracy achievable in predicting Hamiltonians. This dilemma, is also prevalent in other 3D machine learning tasks (Satorras et al., 2021; Batzner et al., 2022; Zitnick et al., 2022; Musaelian et al., 2023) where covariance is considered, besides the task of Hamiltonian modeling, as analyzed by Zitnick et al. 2022.

In this paper, we propose a novel two-stage regression framework to harmonize covariance and expressiveness for Hamiltonian prediction of crystalline materials. The first stage corresponds to a theoretically covariant neural network, such as DeepHE3, constructed based on group theory to model the 3D symmetry of atomic systems and yields an approximate value of the Hamiltonian, with abundant covariant features provided. In the second stage, a highly expressive graph Transformer network we design, with no restrictions on non-linear activations, takes over. This network dynamically learns the 3D structural patterns of the atomic systems, compensates for the expressiveness shortcomings of the first stage network arising from limited non-linear mapping, and refines the Hamiltonian values predicted in the first stage to enhance accuracy. Although this stage forsakes theoretical  $SO(3)$ -equivariance due to its non-linearity, it manages to implicitly capture  $SO(3)$ -equivariance in the learning process through three pivotal mechanisms. First, instead of directly regressing the entire Hamiltonians, the second stage aims to refine the Hamiltonian predictions from the first stage with corrective adjustments. The scope of adjustments is modest, lowering down the difficulties on learning  $SO(3)$ -equivariance of Hamiltonians in a data-driven manner. Second, the second-stage network incorporates covariant features, including  $SO(3)$ -equivariant features from the first-stage network and engineered  $SO(3)$ -invariant features, with its inputs to assist in the implicit learning of  $SO(3)$ -equivariance. Third, as the core of Transformer, the attention mechanism has potentials to adapt to geometric condition variations, including coordinate transformations, through its dynamic weighting strategy. Collectively, the combination of the two stages allows the framework to overcome the limitations of each individual stage and produce precise, generalizable, and covariant predictions.

Our contributions are three-folds:

First, we propose a novel two-stage regression framework that adeptly alleviates the dilemma between expressiveness and covariance in the task of Hamiltonian prediction by designing a complementary combination of a theoretically covariant network and a non-linear network in both representation level and regression target level, thereby ensuring both robust covariance and expressiveness, bringing good accuracy performance with high robustness under coordinate transformations.

Second, we introduce the promising Transformer paradigm (Vaswani et al., 2017) into the DFT Hamiltonian prediction task for crystalline material research by proposing a 3D graph Transformer network in the second stage to refine the predictions of the first-stage network. Through its advanced mechanisms such as covariant feature integration mechanisms as well as multi-head attentions, edge and node features are dynamically encoded and interacted, enabling an effective modeling of diverse 3D atomic systems with covariant properties.

Third, our approach brings a significant improvement in prediction accuracy compared to the state-of-the-art (SOTA) DeepHE3 method across five crystalline material databases, which encompass both strong chemical bonds and weak vdW interactions, and cover different degrees of spin-orbit coupling (SOC), demonstrating the generality of our method for crystalline material research. Moreover, we also surpass the SOTA performance on twisted subsets of the bilayer materials, confirming the good capability of our method on capturing the intrinsic  $SO(3)$ -equivariance of Hamiltonians.

## 2. Related Work

In this part, we firstly overview deep learning studies on capturing rotational equivariance. After that, we segue into related works on deep Hamiltonian prediction, in which 3D rotational equivariance is pursued.

As representative researches on equivariance to discrete rotation group, Dieleman et al. 2016 introduced cyclic symmetry operations into CNNs to achieve rotational equivariance; Ravanbakhsh et al. 2017 explored parameter-sharing techniques for equivariance to discrete rotations; Kondor et al. 2018 developed equivariant representations via compositional methods and tensor theory; Zitnick et al. 2022 and Passaro & Zitnick 2023 used spherical harmonics for atomic modeling, focusing on rotation equivariance but limited to discrete sub-groups of  $SO(3)$  due to their sampling strategy. These approaches were effective for discrete symmetries but not for continuous 3D rotations. Focusing on equivariance to continuous rotation group, Jaderberg et al. 2015 and Cohen & Welling 2017 achieved considerable success in 2D image recognition tasks by modeling equivariance to in-plane rotations. However, their application was limited

within the scope of 2D tasks and did not fit for the more complex demands of equivariance to 3D continuous rotation group, i.e.  $SO(3)$ , in the Hamiltonian prediction task.

In the field of researches on equivariance to  $SO(3)$ , approaches like DeepH (Li et al., 2022) explored equivariance via a local coordinate strategy, which made inference within the fixed local coordinate systems built with neighboring atoms and the output was transformed according to equivariance rules to the corresponding global coordinates. However, due to a lack of in-depth exploration of  $SO(3)$ -equivariance at the network mechanism level, this method was not robust when the local coordinate system underwent rotational disturbances caused by non-rigid deformation, e.g. the interlayer twist of bilayer materials. In contrast, some methods (Thomas et al., 2018; Fuchs et al., 2020; Geiger & Smidt, 2022) considered  $SO(3)$ -equivariance from the perspective of intrinsic mechanisms of neural networks, developed theoretically equivariant tensor operations, such as element-wise multiplication with linear coefficients, direct sum, direct product, as well as the Clebsch-Gordan decomposition, based on the group theory, and have been effectively applied in molecular dynamics modeling (Musaelian et al., 2023) and Hamiltonian prediction (Schütt et al., 2019; Unke et al., 2021; Gong et al., 2023), where DeepHE3 (Gong et al., 2023) was validated as a SOTA method across diverse crystalline materials. However, a common challenge across these methods lies that, to achieve theoretical equivariance, they forbade the use of non-linear mappings for  $SO(3)$ -equivariant features, significantly limiting the network’s expressive potential and creating a bottleneck in generalization performance. Although these approaches tried to enhance expressiveness via a gated activation function, where  $SO(3)$ -invariant features undergone through non-linear activation layers were used to produce gating coefficients that were multiplied with  $SO(3)$ -equivariant features, this mechanism, viewed from the perspective of equivariant features, amounted to a linear operation and did not fundamentally improve their expressive capability. For these methods, this covariance-expressiveness dilemma remains an unsolved problem.

### 3. Preliminary

In the study of symmetry on mathematical structures, covariance encompasses two fundamental concepts: invariance and equivariance. An operation  $A$  is called invariant under another operation  $B$  if the result of  $A$  remains unchanged when  $B$  is applied, formally  $A(B(x)) = A(x)$ ; on the other hand,  $A$  is equivariant with respect to  $B$  if applying  $B$  before or after  $A$  has the same effect, expressed as:  $A(B(x)) = B(A(x))$ . The key covariance properties of Hamiltonians are the 3D translational invariance and rotational equivariance with respect to reference frame. Since

3D translational invariance can be easily achieved in a regression model by using the relative coordinates between two atoms, the focus here should be on studying equivariance to  $SO(3)$ , i.e. a group consisting of all continuous 3D rotation operations. In the context of Hamiltonians, when the reference frame rotates by a rotation matrix denoted as  $\mathbf{R}$ , the edge of an atom pairs  $(i, j)$  transforms from  $\mathbf{r}_{ij}$  to  $\mathbf{R} \cdot \mathbf{r}_{ij}$ , and the Hamiltonians in the direct sum state transforms equivariantly from  $\mathbf{h}_{ij}$  to  $D(\mathbf{R}) \cdot \mathbf{h}_{ij}$ , where  $D(\mathbf{R})$  is the Wigner-D matrix. Note that here we present  $SO(3)$ -equivariance under the direct sum state due to its simple vector form. For the equivalent formulation under the direct product state, please refer to Gong et al. 2023.

The requirements for the fitting and generalization capability of a neural network  $f_{nn}(\cdot)$  for Hamiltonian prediction can be formally expressed as:  $f_{nn}(\{\mathbf{r}_{ij}|i \in Nodes, ij \in Edges\}) \cong \{\mathbf{h}_{ij}\}$ ; moreover, the requirement on  $SO(3)$ -equivariance can be represented as:  $f_{nn}(\{\mathbf{R} \cdot \mathbf{r}_{ij}|i \in Nodes, ij \in Edges\}) \cong \{D(\mathbf{R}) \cdot \mathbf{h}_{ij}\}$ . It is crucial that  $f_{nn}(\cdot)$  intrinsically embodies  $SO(3)$ -equivariance to effectively generalize under rotational reference frames. An intuitive way to achieve this is data-driven learning, however, this is challenging for the Hamiltonian prediction task, since  $\mathbf{h}_{ij} \in \mathbb{R}^{(2l_1+1)+(2l_2+1)\dots+(2l_K+1)}$  is usually high-dimensional, comprising a range of components of different angular momentum, i.e., from  $l_1$  to  $l_K$ . Moreover,  $\mathbf{h}_{ij}$  is not determined in isolation by the types of atom  $i$  and  $j$  as well as their relative positions; geometric of atoms that interact with them also have complex influences on  $\mathbf{h}_{ij}$ . Thus, under rotational operations, the Hamiltonian  $\mathbf{h}_{ij}$  may vary in a vast space, which is difficult to be covered with a finite set of training discrete samples, even with data augmentations. Therefore, it is necessary to consider operators that theoretically maintain  $SO(3)$ -equivariance according to group theory. However, as analyzed in Section 2, this leads to the covariance-expressiveness dilemma, which is the core problem this paper aims to solve.

### 4. Method

As shown in Figure 1, on addressing the covariance-expressiveness dilemma analyzed in previous sections, we propose a novel two-stage cascaded regression framework effectively hybridizing a theoretically guaranteed  $SO(3)$ -equivariant network in the first stage, with a high expressive non-linear network in the second stage from both representation level as well as the regression target level for Hamiltonian prediction in crystalline material research. The network from the first stage provides essential support to the second stage in mastering  $SO(3)$ -equivariance, whereas the network in the second stage enriches the expressive capabilities of the whole framework. The combination of these two stages not only enhances expressiveness but also ensures robust

covariance to coordinate transformations, bringing accurate predictions for Hamiltonians under variant reference frames.

#### 4.1. Initial Features

In our framework, the initial feature for the  $i$  ( $1 \leq i \leq N$ ) th node is its node embedding, denoted as  $\mathbf{z}_i$ , a SO(3)-invariant word vector that marks the type of atom and provides coordinate-independent semantic information. Given the locality of the Hamiltonian (Li et al., 2022), each atom in the local set  $\Omega(i)$  within the cutoff radius of an atom  $i$  form an edge where a Hamiltonian is defined. The initial features for edge  $(i, j)$  include both SO(3)-invariant encodings and SO(3)-equivariant encodings. The former includes edge embeddings  $\mathbf{z}_{ij}$  marking the types of interacting atom pairs, as well as the distance features  $\mathbf{d}_{ij}$  in the form of Gaussian functions (Li et al., 2022); the latter is spherical harmonics (Schrödinger, 1926), denoted as  $Y_l^m(\frac{\mathbf{r}_{ij}}{\|\mathbf{r}_{ij}\|})$ , where  $\frac{\mathbf{r}_{ij}}{\|\mathbf{r}_{ij}\|}$  describes the relative orientation between two atoms. Notably, a node and itself also possess a Hamiltonian. In other words,  $i \in \Omega(i)$  and  $e_{ii}$  also forms a valid edge. In this case,  $Y_l^m(\frac{\mathbf{r}_{ij}}{\|\mathbf{r}_{ij}\|})$  cannot be used to calculate directional features and a vector filled with 0 is used as a substitute.

The above encodings are used as initial features to model the Hamiltonians which obey rotational equivariance. Additionally, they also inherently fulfill translational invariance with respect to global coordinates, another natural attribute of Hamiltonians.

#### 4.2. The First Regression Stage

In our framework, the primary role of the first regression stage is to extract theoretically SO(3)-equivariant node and edge representations, denoted as  $\mathbf{n}_i^{(p)}$  and  $\mathbf{e}_{ij}^{(p)}$  respectively for the  $p$  th ( $1 \leq p \leq P$ ) encoder group, and regress baseline Hamiltonian predictions, denoted as  $\hat{\mathbf{h}}_{ij}$  in the direct sum state and  $\hat{\mathbf{H}}_{ij}$  in the direct product state for each pair  $(i, j)$ , establishing a firm foundation on SO(3)-equivariance in both feature level and the regression target level. We directly choose DeepHE3 as the first-stage network, for two main reasons. First, as an extensively validated SOTA method so far, the node and edge feature encoders in DeepHE3 comprehensively incorporate SO(3)-equivariant tensor operators to aggregate structural features from the local set of a node and then propagate these features outward, enabling equivariant encoding of 3D structural patterns from both local level to larger range. Second, some advanced operations that highly depend on non-linear mappings, such as attention, are difficult to thoroughly perform their SOTA performance with the restrictions on non-linear activation functions imposed by theoretical equivariance in the first stage. Thus, we just take DeepHE3 as the first-stage network and concentrate on developing the second-stage network, where restrictions on non-linear activation are imposed.

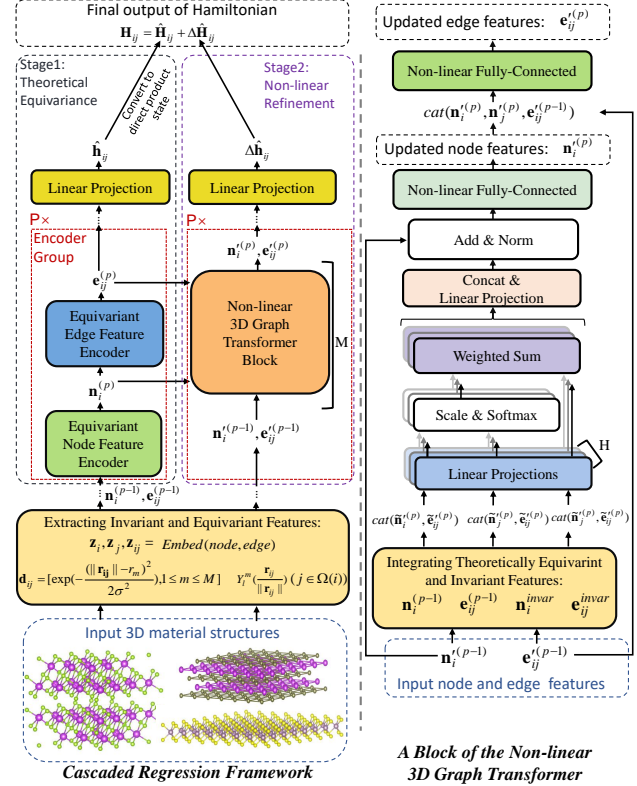


Figure 1. Left part: overview of the two-stage regression framework for Hamiltonian prediction, with the first stage extracting equivariant features and making baseline predictions, and the second stage enhancing accuracy via advanced non-linear networks. The first-stage network aids the second-stage network in learning regression covariance, namely SO(3)-equivariance in this context, and the second-stage network compensates for the expressiveness capability of first-stage network. Right part: The internal architecture of the non-linear 3D graph Transformer network, the core module of the proposed method.

#### 4.3. The Second Regression Stage

The second regression stage of our framework is designed to fully exploit non-linear mappings to enhance the expressive capability of the whole framework. For that purpose, as shown in the right part of Fig. 1, we propose a 3D graph Transformer which effectively models 3D atomic structures and generates non-linear correction terms that complement the predictions from the first stage, achieving high-precision Hamiltonian prediction. Yet, one key problem to solve lies that, non-linear projections might forsake the guarantee on theoretical SO(3)-equivariance of the regression framework, forcing the second-stage network to implicitly capture equivariance through learning from the data. Thus, we must address the difficulty of learning equivariance of Hamiltonians as discussed in Section 3. Our second-stage network adeptly resolves this issue, simultaneously capturing equivariance

and enhancing expressive capabilities. This is primarily attributed to three pivotal mechanisms we design for the second regression stage.

First, in the second regression stage, the prediction target is not the Hamiltonian itself but a correction term  $\Delta\hat{\mathbf{H}}_{ij}$ , relative to the first stage’s output, i.e. the initial Hamiltonian estimate  $\hat{\mathbf{H}}_{ij}$ . The sum of these two stages’ outputs forms the final prediction of the Hamiltonian:  $\mathbf{H}_{ij} = \hat{\mathbf{H}}_{ij} + \Delta\hat{\mathbf{H}}_{ij}$ . Given that the predicted results of  $\hat{\mathbf{H}}_{ij}$  are theoretically SO(3)-equivariant and approximately reasonable, the range of variation for the correction term  $\Delta\hat{\mathbf{H}}_{ij}$ , especially in the context of rotations, becomes smaller compared to  $\hat{\mathbf{H}}_{ij}$ . This reduces the complexity of the output space for the second stage and enhances the feasibility of implicitly capturing SO(3)-equivariance through data-driven learning.

Second, the theoretically covariant features, including both SO(3)-equivariant and SO(3)-invariant features, are integrated into the input node and edge features of each Transformer block in the second stage to aid it in capturing equivariance, as shown in Eq. (1):

$$\begin{aligned}\tilde{\mathbf{n}}_i^{(p)} &= \mathbf{n}_i^{(p-1)} + \alpha \mathbf{n}_i^{(p-1)} + \beta \mathbf{n}_i^{invar} \\ \tilde{\mathbf{e}}_{ij}^{(p)} &= \mathbf{e}_{ij}^{(p-1)} + \lambda \mathbf{e}_{ij}^{(p-1)}\end{aligned}\quad (1)$$

where  $\alpha$ ,  $\beta$  and  $\lambda$  are hyperparameters,  $\mathbf{n}_i^{(p-1)}$  and  $\mathbf{e}_{ij}^{(p-1)}$  denote the outputs of the Transformer at the  $p-1$  th encoder group,  $\tilde{\mathbf{n}}_i^{(p)}$  and  $\tilde{\mathbf{e}}_{ij}^{(p)}$  respectively serve as the input node and edge features for the subsequent modules of the  $p$  th encoder group,  $\mathbf{n}_i^{(p-1)}$  and  $\mathbf{e}_{ij}^{(p-1)}$  are the SO(3)-equivariant node and edge features, correspondingly, from the  $p-1$  th encoder group of the first-stage network. Besides SO(3)-equivariant features, since as demonstrated by literature (Wang et al., 2018; Zhang et al., 2019; Zhang & Jiang, 2023), SO(3)-invariant features also facilitate the learning of SO(3)-equivariance, we also develop a SO(3)-invariant node feature, i.e.,  $\mathbf{n}_i^{invar}$ , aggregated from multiple SO(3)-invariant features, such as node embeddings  $\mathbf{z}_i$ , edge embeddings  $\mathbf{z}_{ij}$ , distance features  $\mathbf{d}_{ij}$ , and triplet angle feature  $\theta_{ijk}$  formed by node  $i$  as well as two of its neighboring atoms  $j$  and  $k$ , in the way like:

$$\mathbf{n}_i^{invar} = \sum_{(j,k) \in \Omega(i)} FC(\text{cat}(\mathbf{z}_i, \mathbf{z}_j, \mathbf{z}_k, \mathbf{d}_{ij}, \mathbf{d}_{ik}, \mathbf{c}_{ijk}))\quad (2)$$

where  $\text{cat}(\cdot)$  is the concatenation operator,  $FC(\cdot)$  denotes fully-connected layers with non-linear activations,  $\mathbf{c}_{ijk} = [\cos(\theta_{ijk}), \cos(\theta_{ijk}), \dots]$  is a vector extended by duplication, which serves to amplify the angle features for  $FC(\cdot)$ . We partition the set  $\Omega(i)$  into distinct tuples  $(j, k)$ , without node overlap among different tuples, to efficiently compute  $\mathbf{n}_i^{invar}$ . In Eq. (1),  $\mathbf{n}_i^{invar}$  is directly merged into node features, and since node features are then merged into

edge features in the subsequent modules, it also enhances in the learning of edge features. With the help of the collection of theoretically covariant features, the second-stage network, even a non-linear one, can better capture the SO(3)-equivariant properties inherent in the Hamiltonian.

Third, as the core of the Transformer, we design a potent multi-head attention mechanism to learn node and edge representations of the 3D atom system. The capability to dynamically focus on related geometric features equips it with robust adaptability for diverse geometric conditions, from structural variants to coordinate transformations. Specifically, the attention mechanism firstly learns dynamic weights, i.e.  $\alpha_{ij}^{(p)}$  for the edge  $(i, j)$  at the  $p$  th encoder group, based on the interactive relationship between the current atom  $i$  and its local atoms  $j \in \Omega(i)$ , as shown in Eq. (3):

$$\begin{aligned}\mathbf{q}_{ij}^{h(p)} &= \mathbf{W}_q^h \cdot \text{cat}(\tilde{\mathbf{n}}_i^{(p)}, \tilde{\mathbf{e}}_{ij}^{(p)}), \\ \mathbf{k}_{ij}^{h(p)} &= \mathbf{W}_k^h \cdot \text{cat}(\tilde{\mathbf{n}}_j^{(p)}, \tilde{\mathbf{e}}_{ij}^{(p)}) \\ \alpha_{ij}^{(p)} &= \text{softmax}\left(\frac{(\mathbf{q}_{ij}^{h(p)})^T \cdot \mathbf{k}_{ij}^{h(p)}}{\sqrt{d_h}}\right)\end{aligned}\quad (3)$$

where  $h(1 \leq h \leq H)$  is the head index,  $d_h$  is the dimension of  $\mathbf{q}_{ij}^{h(p)}$  and  $\mathbf{k}_{ij}^{h(p)}$ ,  $\mathbf{W}_q^h$  and  $\mathbf{W}_k^h$  are parameter matrices to calculate queries and keys, respectively. Here the scale factor  $\sqrt{d_h}$  in the denominator is used to prevent  $\text{softmax}(\cdot)$  from gradient saturation, and the multiple heads aim at enchaining the model capacity. Based on  $\alpha_{ij}^{(p)}$ , the node features are updated flexibly through the structural information embedded in its local sets, as shown in Eq. (4):

$$\begin{aligned}\mathbf{v}_i^{h(p)} &= \sum_{j \in \Omega(i)} \alpha_{ij}^{(p)} \cdot (\mathbf{W}_v^h \cdot \text{cat}(\tilde{\mathbf{n}}_j^{(p)}, \tilde{\mathbf{e}}_{ij}^{(p)})), \\ \mathbf{n}_i^{(p)} &= FC(LN(\mathbf{W}_o \cdot \text{cat}(\mathbf{v}_i^{1(p)}, \dots, \mathbf{v}_i^{H(p)}) + \mathbf{n}_i^{(p-1)}))\end{aligned}\quad (4)$$

where  $LN(\cdot)$  denotes the layer normalization operator,  $FC(\cdot)$  here denotes fully-connected layers with non-linear activations. Based on  $\mathbf{n}_i^{(p)}$ , the edge representations are updated as:

$$\mathbf{e}_{ij}^{(p)} = FC(\text{cat}(\mathbf{n}_i^{(p)}, \mathbf{n}_j^{(p)}, \mathbf{e}_{ij}^{(p-1)}))\quad (5)$$

when repeatedly stacking operations in Eq. (4) and (5) in an alternate manner, local patterns can incrementally spread to a larger scale through the neighbors of neighboring atoms. Nevertheless, given the Hamiltonian’s locality, there’s typically no need for information transfer over long distances. Finally, the correction term outputted by the second stage is regressed from the edge features  $\mathbf{e}_{ij}^{(p)}$  encoded by its last layer of the encoder, in the way like:

$$\Delta\hat{\mathbf{H}}_{ij} = DStoDP(\Delta\hat{\mathbf{h}}_{ij}) = DStoDP(FC(\mathbf{e}_{ij}^{(p)}))\quad (6)$$

where  $DStoDP(\cdot)$  is the conversion operation from the direct sum state to the direct product state, which is more commonly used in the down-stream computational tasks based on Hamiltonians.

#### 4.4. Training

Considering that networks from the two stages employ fundamentally different operators, training them simultaneously in a joint manner may pose optimization difficulties. Therefore, we optimize them separately. In the first phase, parameters of the first stage network are optimized by minimizing  $MSE(\mathbf{H}_{ij}^* - \hat{\mathbf{H}}_{ij})$ , while in the second phase, parameters of the second stage network are optimized by minimizing  $MSE((\mathbf{H}_{ij}^* - \hat{\mathbf{H}}_{ij}) - \Delta\hat{\mathbf{H}}_{ij})$ . To avoid interference, the two-stage networks use independent node and edge embeddings. Moreover, during the training of the second stage network, gradients are not propagated back to the first-stage network. Adam is used for optimization.

### 5. Discussion on Time Complexity

The time Complexity for both of the first-stage and the second-stage networks are  $\mathcal{O}(BNE)$ , where  $B$  is the number of their basic blocks,  $N$  is the total number of atoms in a system,  $E$  is the average number of atoms within the cutoff radius of a given atom. Due to the locality of the Hamiltonian, for a given class of atomic systems,  $E$  is roughly a constant and does not significantly increase with the growth of  $N$ . Therefore, for big atomic systems with very large  $N$ ,  $E \ll N$ , and similarly,  $B \ll N$ . In this case, the time complexity of our framework tends towards  $\mathcal{O}(N)$ . In contrast, for traditional DFT method (Kohn & Sham, 1965), which requires  $T$  rounds of iterative decomposition of  $N \times N$  matrices, the time complexity is  $\mathcal{O}(TN^3)$ . As  $N$  increases, the cubic complexity of  $N$  results in significant computational overhead, and to achieve self-consistency,  $T$  is usually very large, exacerbating the computational burden, leading to the difficulties for simulations of large atomic systems within an acceptable time frame. On the contrary, our framework offers an efficient pathway for simulating large atomic systems with linear time complexity of  $N$  and without the need for  $T$  rounds of iterations.

## 6. Experiments

### 6.1. Experimental Conditions

We conduct experiments on five crystalline material databases, including Monolayer Graphene (abbreviated as *MG*), Monolayer MoS2 (*MM*), Bilayer Bismuthene (*BB*), Bilayer Bi2Te3 (*BT*), and Bilayer Bi2Se3 (*BS*), which are released by the DeepH series (Li et al., 2022; Gong et al., 2023). These databases exhibit both diversity and representativeness, as they encompass materials with strong chemi-

Table 1. Statistics of experimental databases, detailing the sizes of training, validation, and testing set including both non-twisted samples (NT) and twisted samples (T), as well as the dimension of the Hamiltonian for each atom pair. Note that  $\text{Dim}(\mathbf{H}_{ij}) = \text{Dim}(\mathbf{h}_{ij})$  when flattened.

	MG	MM	BB	BT	BS
TRAIN (NT)	270	300	231	204	231
VAL (NT)	90	100	113	38	113
TEST (NT)	90	100	113	12	113
TEST (T)	-	-	4	2	2
Dim( $\mathbf{h}_{ij}$ )	361		2888		

cal bonds within individual layers and weak vdW interactions between layers; and include materials exhibiting varied degrees of spin-orbit coupling (SOC), featuring both strong SOC examples like *BT*, *BB* and *BS*, as well as others with weak SOC. These materials have wide application potentials in electronic devices, energy equipments, and quantum components. The training, validation, and test sets we use for each database are exactly the same as DeepHE3, and details of these databases are shown in Table 1. Notably, for materials with bilayer structures, apart from their primary test sets without overall rotations between the two layers, the DeepH series also offered a small number of samples featuring two layers relatively twisted to each other, since twisted structures have become a research hotspot due to their potential for new electrical and quantum topological properties (Cao et al., 2018; Park et al., 2021; Ferreira, 2022). During such non-rigid transformations, the established coordinate system, defined by one layer’s lattice vectors, undergoes rotations to the other layer. These twisted subsets are challenging because there are no direct twisted samples in the training set; the network has to profoundly capture the intrinsic  $\text{SO}(3)$ -equivariance of the system to reasonably extrapolate the Hamiltonian under such rotational behavior.

The Mean Absolute Error (MAE) metric is used as the accuracy metric. Besides the classical MAE metric, denoted as  $MAE_{all}$ , for measuring the average error among all testing samples, the MAE on the most challenging sample with worst accuracy from each database is also a crucial metric. We record this metric as well and denote it as  $MAE_{cha}$ , to distinguish it from  $MAE_{all}$ . To ensure the reproducibility of our experimental results, we follow DeepHE3 to use a fixed random seed, i.e., 42, for model initialization and random sampling in the dataloader. To further offset the randomness of experiments, we conduct independent experiments for 10 times repeatedly and report  $MAE_{all}$  and  $MAE_{cha}$ , averaged across these 10 experiments. Additionally, we report the standard deviation ( $\pm\sigma$ ), a bar measuring the statistical fluctuation of the experimental results. To facilitate the implicit learning of the  $\text{SO}(3)$ -equivariance of Hamiltonians for the non-linear parts of our framework, we

Table 2. Comparison of experimental results on five material databases and the twisted subsets. For bilayer structures, the superscripts  $nt$  and  $t$  denote the non-twisted and twisted testing samples, respectively. Both the mean and standard deviation of  $MAE_{cha}$  as well as  $MAE_{all}$  (meV) from 10 independent repeated experiments are provided.

DATASET	METHOD	$MAE_{all}$	$MAE_{cha}$
MG	DEEPHE3	0.260 ± 0.002	0.576 ± 0.002
	OURS	<b>0.179 ± 0.001</b>	<b>0.469 ± 0.001</b>
MM	DEEPHE3	0.410 ± 0.002	1.532 ± 0.003
	OURS	<b>0.233 ± 0.001</b>	<b>0.520 ± 0.002</b>
BB <sup>nt</sup>	DEEPHE3	0.257 ± 0.002	1.652 ± 0.002
	OURS	<b>0.172 ± 0.001</b>	<b>0.973 ± 0.002</b>
BT <sup>nt</sup>	DEEPHE3	0.447 ± 0.001	2.410 ± 0.003
	OURS	<b>0.294 ± 0.002</b>	<b>1.723 ± 0.002</b>
BS <sup>nt</sup>	DEEPHE3	0.399 ± 0.003	1.556 ± 0.001
	OURS	<b>0.282 ± 0.002</b>	<b>1.244 ± 0.002</b>
BB <sup>t</sup>	DEEPHE3	0.468 ± 0.003	0.602 ± 0.004
	OURS	<b>0.438 ± 0.003</b>	<b>0.578 ± 0.025</b>
BT <sup>t</sup>	DEEPHE3	0.831 ± 0.003	0.850 ± 0.003
	OURS	<b>0.774 ± 0.002</b>	<b>0.794 ± 0.003</b>
BS <sup>t</sup>	DEEPHE3	0.370 ± 0.001	0.390 ± 0.002
	OURS	<b>0.345 ± 0.002</b>	<b>0.367 ± 0.001</b>

introduce rigid rotational data augmentation on the samples during training. Our experiments are conducted on an internal cluster of Tesla A100 servers where each card has 80 GiB of GPU memory.

Regarding hyperparameter selection, to ensure fairness in comparison, for the first stage network (DeepHE3), we use the same hyperparameters as those gathered in its latest open-source project<sup>1</sup>. For the Transformer network we propose in the second regression stage, we conduct hyperparameter selection according to the  $MAE_{all}$  performance on the validation sets. The hyperparameters that need to be determined include: the number of Transformer blocks ( $W$ ) within one encoder group  $p$  ( $1 \leq p \leq P$ ), where  $P$  is set as 3 in advance to align with DeepHE3; the number of heads ( $H$ ) in the multi-attention mechanism; the coefficients ( $\alpha, \beta, \lambda$ ) for feature fusion in Eq. (3); as well as the learning rate  $\gamma$  and batch size ( $B$ ) for training. They are searched from:  $1 \leq W \leq 6$ ,  $\alpha, \beta, \lambda \in \{0.0, 0.1, \dots, 1.5\}$ ,  $\gamma \in \{1 * 10^{-4}, 2 * 10^{-4}, \dots, 1 * 10^{-3}\}$ ,  $1 \leq B \leq 5$ . A coarse-to-fine grid search for hyperparameters is conducted, and we select the minimum value for each hyperparameter at which further increasing its value does not lead to a significant improvement ( $p.value < 0.05$ ) on the validation sets. Their optimal values identified through this search are as follows:  $W^* = 4$ ,  $\alpha^* = 0.8$ ,  $\beta^* = 0.9$ ,  $\lambda^* = 0.4$ ,  $\gamma^* = 3 * 10^{-4}$ ,  $B^* = 2$ . It can be seen that the network

architecture we adopted is not very deep, which matches the scale of the training sets. Notably, although our method is independently trained on the training set of each individual material database, to obtain a set of general hyperparameters, the overall performance across the validation sets of different materials is considered to select hyperparameters. After hyperparameter selection, our method is retrained on each individual training set according to the optimal hyperparameters and the best epoch on its validation set is outputted for testing.

## 6.2. Experimental Results and Analysis

We compare DeepHE3 with the proposed method (denoted as Ours) in Table 2 on the five material databases as well as the corresponding twisted subsets. The results of DeepHE3 are derived from our reproduction experiments through the script collection for one-click reproduction from their latest open source resources<sup>1</sup>, a little bit better than that reported in their original paper (Gong et al., 2023).

From Table 2, we could observe that the superior accuracy of our method across five databases, significantly outperforming DeepHE3. Specifically, on  $MG$ ,  $MM$ ,  $BB^{nt}$ ,  $BT^{nt}$  and  $BS^{nt}$ , we respectively lower down  $MAE_{all}$  by a relative ratio of 31.15%, 43.17%, 33.07%, 34.22%, and 29.32%, respectively, and lower down  $MAE_{cha}$  by 18.57%, 66.06%, 41.10%, 28.13%, and 20.05%, correspondingly, compared to DeepHE3. This indicates that our method excels in accuracy, both on average and for the most challenging samples. This is attributed to that, DeepHE3, on ensuring theoretical symmetry, limits the use of non-linear activation functions, leading to a constrained expressive capability and consequently, a bottleneck in generalization performance. To solve this, we extend it to a two-stage regression framework. Through introducing a non-linear network, i.e. a 3D graph Transformer with good potentials of generalizing the diverse geometric conditions via several advanced non-linear mechanisms, we significantly enhance the expressive capability of the regression framework, fully capturing the complexity of Hamiltonians. Furthermore, experimental results on the twisted subsets, namely  $BB^t$ ,  $BT^t$  and  $BS^t$ , illustrates the robust generalization capability of our method to reference frame rotations caused by inter-layer twists. Combining with Table 1, it can be seen that the Hamiltonian of each pair of atoms is high-dimensional. For nonlinear operators without the theoretical guarantee on symmetry, it is challenging to capture their  $SO(3)$ -equivariance in such a large space and produce high generalization performance with respect to variant reference frames. Yet, as demonstrated in Table 2, our framework can well handle this challenge and achieve remarkable prediction accuracy. We outperform DeepHE3 by decreasing the  $MAE_{all}$  metric with a ratio of

<sup>1</sup><https://github.com/Xiaoxun-Gong/DeepH-E3>

6.41%, 6.86%, and 6.76%, and the  $MAE_{cha}$  metric with a ratio of 3.98%, 6.59%, and 5.90%, on the respective subsets. These results demonstrate that, despite the extensive use of non-linear operators, our framework can well capture the  $SO(3)$ -equivariance properties of Hamiltonians with the help of covariant mechanisms from the first regression stage, and accurately generalizes across variant coordinate systems

Among current deep learning-based studies on Hamiltonians modeling, only the DeepH series have conducted comprehensive experiments on various properties of crystalline materials, proving SOTA performance. In the paper of DeepHE3, it is proven to surpass DeepH (Li et al., 2022) in accuracy, as the latter didn't consider covariance at the network mechanism level; and since our method further outperforms DeepHE3 in accuracy, we may conclude that our work represents the new SOTA in the field of deep learning research for Hamiltonian prediction on crystal material analysis.

## 7. Conclusion

In crystalline material research, deep learning for Hamiltonian regression requires adherence to covariance laws, a pivotal challenge being the achievement of  $SO(3)$ -equivariance without compromising network expressiveness, due to the limitations of non-linear mappings in assuring theoretical equivariance. To address this, we propose a two-stage cascaded regression framework, where the stage employs a theoretically-informed covariant neural network for modeling the covariant properties of 3D atomic structures, yielding baseline Hamiltonians with series of covariant features assisting the subsequent stage on capturing  $SO(3)$ -equivariance. The second stage, leverages the proposed non-linear 3D graph Transformer network for fine-grained structural analysis of 3D atomic systems, refining the initial Hamiltonian predictions via enhanced network expressiveness. Such a combination allows for accurate, generalizable Hamiltonian predictions while upholding strong covariance against coordinate transformations. Our methodology demonstrates SOTA performance in Hamiltonian prediction, validated through five crystalline material databases.

## References

- Batzner, S., Musaelian, A., Sun, L., Geiger, M., Mailoa, J. P., Kornbluth, M., Molinari, N., Smidt, T. E., and Kozinsky, B. E (3)-equivariant graph neural networks for data-efficient and accurate interatomic potentials. *Nature Communications*, 13(1):2453, 2022.
- Cao, Y., Fatemi, V., Fang, S., Watanabe, K., Taniguchi, T., Kaxiras, E., and Jarillo-Herrero, P. Unconventional superconductivity in magic-angle graphene superlattices. *Nature*, 556(7699):43–50, 2018.
- Cohen, T. S. and Welling, M. Steerable cnns. In *ICLR*, 2017.
- Dieleman, S., Fauw, J. D., and Kavukcuoglu, K. Exploiting cyclic symmetry in convolutional neural networks. In *ICML Workshop*, volume 48, pp. 1889–1898, 2016.
- Ferreira, F. Multiscale modelling of twisted bilayers of 2d materials. *Nature Reviews Physics*, 4(10):632–632, 2022.
- Fuchs, F., Worrall, D. E., Fischer, V., and Welling, M. Se(3)-transformers: 3d roto-translation equivariant attention networks. In *NeurIPS*, 2020.
- Geiger, M. and Smidt, T. E. e3nn: Euclidean neural networks. *CoRR*, abs/2207.09453, 2022.
- Gong, X., Li, H., Zou, N., Xu, R., Duan, W., and Xu, Y. General framework for e (3)-equivariant neural network representation of density functional theory hamiltonian. *Nature Communications*, 14(1):2848, 2023.
- Gu, Q., Zhang, L., and Feng, J. Neural network representation of electronic structure from ab initio molecular dynamics. *Science Bulletin*, 67(1):29–37, 2022.
- Hohenberg, P. and Kohn, W. Inhomogeneous electron gas. *Physical Review*, 136(3B):B864, 1964.
- Jaderberg, M., Simonyan, K., Zisserman, A., and Kavukcuoglu, K. Spatial transformer networks. In *NeurIPS*, pp. 2017–2025, 2015.
- Kohn, W. and Sham, L. J. Self-consistent equations including exchange and correlation effects. *Physical Review*, 140(4A):A1133, 1965.
- Kondor, R., Son, H. T., Pan, H., Anderson, B. M., and Trivedi, S. Covariant compositional networks for learning graphs. In *ICLR Workshop*, 2018.
- Li, H., Wang, Z., Zou, N., Ye, M., Xu, R., Gong, X., Duan, W., and Xu, Y. Deep-learning density functional theory hamiltonian for efficient ab initio electronic-structure calculation. *Nature Computational Science*, 2(6):367–377, 2022.
- Musaelian, A., Batzner, S., Johansson, A., Sun, L., Owen, C. J., Kornbluth, M., and Kozinsky, B. Learning local equivariant representations for large-scale atomistic dynamics. *Nature Communications*, 14(1), 2023.
- Park, J. M., Cao, Y., Watanabe, K., Taniguchi, T., and Jarillo-Herrero, P. Tunable strongly coupled superconductivity in magic-angle twisted trilayer graphene. *Nature*, 590(7845):249–255, 2021.



- Passaro, S. and Zitnick, C. L. Reducing  $SO(3)$  convolutions to  $SO(2)$  for efficient equivariant gnns. In *ICML*, pp. 27420–27438, 2023.
- Ravanbakhsh, S., Schneider, J. G., and Póczos, B. Equivariance through parameter-sharing. In *ICML*, pp. 2892–2901, 2017.
- Satorras, V. G., Hoogeboom, E., and Welling, M.  $E(n)$  equivariant graph neural networks. In *ICML*, volume 139, pp. 9323–9332, 2021.
- Schrödinger, E. Quantisierung als eigenwertproblem. *Annalen der Physik*, 384(4):361–376, 1926.
- Schütt, K. T., Gastegger, M., Tkatchenko, A., Müller, K.-R., and Maurer, R. J. Unifying machine learning and quantum chemistry with a deep neural network for molecular wavefunctions. *Nature Communications*, 10(1):5024, 2019.
- Thomas, N., Smidt, T., Kearnes, S., Yang, L., Li, L., Kohlhoff, K., and Riley, P. Tensor field networks: Rotation-and translation-equivariant neural networks for 3d point clouds. *arXiv preprint arXiv:1802.08219*, 2018.
- Unke, O., Bogojeski, M., Gastegger, M., Geiger, M., Smidt, T., and Müller, K.-R. Se (3)-equivariant prediction of molecular wavefunctions and electronic densities. volume 34, pp. 14434–14447, 2021.
- Vaswani, A., Shazeer, N., Parmar, N., Uszkoreit, J., Jones, L., Gomez, A. N., Kaiser, L., and Polosukhin, I. Attention is all you need. In *NeurIPS*, pp. 5998–6008, 2017.
- Wang, H., Zhang, L., Han, J., and Weinan, E. Deepmd-kit: A deep learning package for many-body potential energy representation and molecular dynamics. *Computer Physics Communications*, 228:178–184, 2018.
- Zhang, Y. and Jiang, B. Universal machine learning for the response of atomistic systems to external fields. *Nature Communications*, 14, 2023.
- Zhang, Y., Hu, C., and Jiang, B. Embedded atom neural network potentials: Efficient and accurate machine learning with a physically inspired representation. *The journal of physical chemistry letters*, 10(17):4962–4967, 2019.
- Zitnick, L., Das, A., Kolluru, A., Lan, J., Shuaibi, M., Sriram, A., Ulissi, Z. W., and Wood, B. M. Spherical channels for modeling atomic interactions. In *NeurIPS*, 2022.